Journal of Nuclear Medicine, published on October 4, 2019 as doi:10.2967/jnumed.119.229781

First-in-human imaging with ^{89}Zr-Df-IAB22M2C anti-CD8 minibody in patients with solid malignancies: preliminary pharmacokinetics, biodistribution, and lesion targeting

Neeta Pandit-Taskar[1,2,3], Michael A. Postow[4,5], Matthew D. Hellmann[3,4,5], James J. Harding[4,5], Christopher A. Barker[6], Joseph A. O'Donoghue[7], Martha Ziolkowska[1], Shutian Ruan[1,2], Serge K. Lyashchenko[8,9], Frank Tsai[10], Michael Farwell[11], Tara C. Mitchell[11], Ron Korn[12], William Le[13], Jason S. Lewis[1,8,9], Wolfgang A. Weber[1] , Deepak Behera[13], Ian Wilson[13], Michael Gordon[10], Anna M. Wu[13,14], Jedd D. Wolchok[3,4,5]

[1]Department of Radiology, Memorial Sloan Kettering Cancer Center, New York, NY
[2]Department of Radiology, Weill Cornell Medical College, New York, NY
[3]Parker Institute for Cancer Immunotherapy, Memorial Sloan Kettering Cancer Center, New York, NY
[4]Department of Medicine, Memorial Sloan Kettering Cancer Center, New York, NY
[5]Department of Medicine, Weill Cornell Medical College, New York, NY
[6]Department of Radiation Oncology, Memorial Sloan Kettering Cancer Center, New York, NY
[7]Department of Medical Physics, Memorial Sloan Kettering Cancer Center, New York, NY
[8]Molecular Pharmacology Program, Memorial Sloan Kettering Cancer Center, New York, NY
[9]Radiochemistry & Molecular Imaging Probes Core, Memorial Sloan Kettering Cancer Center, New York, NY
[10]Honor Health, Scottsdale, AZ
[11]University of Pennsylvania, Philadelphia, PA
[12]Imaging Endpoints, Scottsdale, AZ
[13]ImaginAb, Inc., Inglewood, CA
[14]Department of Molecular Imaging and Therapy, Beckman Research Institute of the City of Hope, Duarte CA

Corresponding author:

Neeta Pandit-Taskar, MD

Memorial Sloan Kettering Cancer Center

1275 York Avenue

New York, NY 10065

pandit-n@mskcc.org

Running title: Anti CD8 89Zr-IAB22M2C minibody PET

Research support: This research was supported by ImaginAb, Inc., the Parker Institute for Cancer Immunotherapy, and the Radiochemistry & Molecular Imaging Probe Core of MSK, supported by NIH/NCI Cancer Center Support Grant P30 CA008748.

Word count: 5,552

ABSTRACT

Immunotherapy is becoming the mainstay for treatment of a variety of malignancies, but only a subset of patients respond to treatment. Tumor-infiltrating CD8-positive (CD8+) T lymphocytes play a central role in anti-tumor immune responses. Non-invasive imaging of CD8+ T cells may provide new insights into the mechanisms of immunotherapy and potentially predict treatment response. We are studying the safety and utility of ^{89}Zr-IAB22M2C, a radiolabeled minibody against CD8+ T cells, for targeted imaging of CD8+ T cells in patients with cancer. **Methods:** The intial dose escalation phase of this first-in-human prospective study included 6 patients (melanoma, 1; lung, 4; HCC, 1). Patients received approximately 111 MBq (3 mCi) of ^{89}Zr-IAB22M2C (at minibody mass doses of 0.2, 0.5, 1.0, 1.5, 5, or 10 mg) as a single dose, followed by PET/CT scans at ~1-2, 6-8, 24, 48, and 96–144 h post-injection (p.i.). Biodistribution in normal organs, lymph nodes, and lesions was evaluated. In addition, serum samples were obtained at ~5, 30, and 60 min and later at the times of imaging. Patients were monitored for safety during infusion and up to the last imaging time point. **Results:** ^{89}Zr-IAB22M2C infusion was well tolerated with no immediate or delayed side effects observed after injection. Serum clearance was typically bi-exponential and dependent on the mass of minibody administered. Areas under the serum time-activity curve normalized to administered activity ranged from 1.3 h/l for 0.2 mg to 8.9 h/l for 10 mg. Biodistribution was dependent

on the minibody mass administered. The highest uptake was always seen in spleen, followed by bone marrow. Liver uptake was more pronounced with higher minibody masses. Kidney uptake was typically low. Prominent uptake was seen in multiple normal lymph nodes as early as 2 h p.i., reaching peak levels by 24–48 h p.i. Uptake in tumor lesions was seen on imaging as early as 2 h p.i., with a majority of ^{89}Zr-IAB22M2C-positive lesions detectable by 24 h. Lesions were visualized early in patients receiving treatment, with SUV ranging from 5.85–22.8 in 6 target lesions. **Conclusions:** ^{89}Zr-IAB22M2C imaging is safe and has favorable kinetics for early imaging. Biodistribution suggests successful targeting of CD8+ T cell-rich tissues. The observed targeting of tumor lesions suggests this may be informative for CD8+ T cell accumulation within tumors. Further evaluation is underway.

Key Words: ^{89}Zr-IAB22M2C PET, minibody, CD8+ T cell, lung cancer, melanoma

INTRODUCTION

Immunotherapy with checkpoint inhibitors has recently emerged as a useful treatment for a variety of solid tumors and select hematologic malignancies. The goals of immunotherapy include recruiting or increasing the activation of immune cells to enhance tumor killing. Tumor-infiltrating T cells (TIL) play a central role in this process (*1*) and, in particular, those composed of CD8+ T cells are important for initiating and mediating a response to CTLA-4 and anti-PD-1/PD-L1 checkpoint inhibitors (*2-5*). Although treatment with checkpoint inhibitors can be effective, responses are only seen in a subset of patients (*6, 7*). Therefore, effective methods to select effective therapies and predict response would play a critical role in patient management. In particular, the ability to non-invasively visualize CD8+ T cells *in vivo* before and during treatment would represent a major advancement in our understanding of local and systemic immune responses and facilitate the development of more effective immune cell-targeted single or combination therapies.

IAB22M2C is an 80 kDa minibody (engineered scFv-C_H3 antibody fragment) with high affinity to human CD8. IAB22M2C is a bivalent homodimer with each monomer consisting of a single-chain variable fragment (scFv) linked to the human IgG1 CH3 domain engineered from the humanized heavy and light chain sequences of murine anti-human OKT8 antibody, and targets human CD8 with high affinity (binding EC50 = 0.4 nM). The minibody is fully humanized and

lacks a C_H2 domain, resulting in a protein that is biologically inert and therefore does not interact with Fc-gamma receptors or the FcRn recycling receptor. Combined with the reduced molecular weight of the minibody, these modifications produce an antibody fragment with accelerated serum clearance, favorable for *in vivo* imaging (*8, 9*).

Preclinical studies of IAB22M2C and desferrioximine-conjugated IAB22M2C showed retention of high-affinity binding to human T cells and HPBALL leukemia cells. Incubation with peripheral blood mononuclear cells (PBMCs) from healthy human donors showed no measurable impact on proliferation or depletion of CD8+ T cells, nor induction of cytokines when donor cells were exposed to immobilized protein. *In vivo* studies in humanized NSG mice engrafted with CD34+ stem cells showed no acute effects of Df-IAB22M2C on CD8+ T cell populations nor cytokine release following intravenous administration. For full-size antibodies, optimal lesion detection typically occurs 4-8 days after injection (*10*). Smaller sized minibodies have faster clearance, leading to high tumor-to-background ratios at earlier times and the feasibility of early imaging (*11-13*).

Df-IAB22M2C was radiolabeled with ^{89}Zr for immunoPET studies in a humanized mouse model of graft-vs-host disease, demonstrating the ability to visualize infiltrating human CD8+ T cells in affected organs (*14*). These and other

studies supported the successful filing of an IND for cGMP manufactured and labeled ^{89}Zr-Df-IAB22M2C for clinical evaluation.

Here we provide a preliminary report on this first-in-human evaluation of ^{89}Zr-IAB22M2C imaging in the first six patients with solid tumors who were either undergoing or likely to undergo immunotherapy.

MATERIALS AND METHODS

A prospective Phase I, open-label, non-randomized, dose escalation imaging study with ^{89}Zr-IAB22M2C was performed in patients with various malignancies. Eligible tumors included small cell or non-small cell lung cancer, squamous cell carcinoma of head and neck, melanoma, Merkel cell carcinoma, renal cell carcinoma, bladder cancer, hepatocellular carcinoma, triple-negative breast cancer, gastroesophageal cancers, and Hodgkin's lymphoma. The protocol was Institutional Review Board-approved, and all patients provided written informed consent (ClinicalTrials.gov identifier NCT03107663).

All patients had histologically confirmed malignancies with at least one measurable lesion and were either on immunotherapy or were eligible to receive immunotherapy. All underwent baseline imaging, including CT and/or MRI performed as standard of care within four weeks of ^{89}Zr-IAB22M2C administration. The total IAB22M2C mass dose was escalated, starting with 0.2 mg and increasing to 0.5, 1.0, 1.5, 5.0, and 10 mg in one patient each

consecutively for the first six patients. All patients underwent serial imaging for biodistribution and multiple blood sampling for pharmacokinetic analysis.

^{89}Zr-IAB22M2C Minibody Formulation and Injection

IAB22M2C minibody, obtained from ImaginAb, Inc. (Inglewood, CA), was conjugated to GMP-grade DFO from Macrocyclics (Dallas, TX) in the Radiochemistry and Molecular Imaging Core facility at MSK (New York, NY). Sterile Df-IAB22M2C was stored at 4°C for up to two weeks before radiolabeling. ^{89}Zr production and subsequent radiolabeling of Df-IAB22M2C were performed as previously described (*15-17*). Approximately 0.2–1 mg of Df-IAB22M2C was labeled with ^{89}Zr and purified by PD-10 column. The final product was supplemented with cold IAB22M2C minibody and diluted with formulation buffer, as needed. The final radiolabeled product was tested pre-release for appearance, pH, radiochemical identity, and purity by size exclusion, high-performance liquid chromatography (SE-HPLC), instant thin layer chromatography (iTLC), radionuclidic purity by gamma spectroscopy, endotoxin level by portable test system (PTS) reader, and immunoreactivity by bead method. Sterility testing was performed post-release. The radiolabeling efficiency was >80%, radiochemical purity was >95%, as determined by iTLC, and minibody binding was >90%.

^{89}Zr-IAB22M2C Administration

The radiolabeled minibody, in combination with cold Df-IAB22M2C to make up the designated total mass balance, was administered IV over 5–10 minutes. No premedications were administered. Patients were monitored for vital signs and any side effects up to the time of imaging (2–4 h or 6–8 h p.i.) on the day of injection, and 24 h later for any reactions or adverse events; side effects and reactions were graded per CTCAE version 4.0 criteria.

PET Imaging

Images were acquired at two centers using either a GE Discovery 710 PET/CT scanner or a GE Discovery STE PET/CT scanner. Each patient underwent 4-5 whole-body PET/CT scans from vertex of the skull to feet at 2-4 h, 24 ± 4 h, 48 ± 4 h, and 92–148 h p.i. Patients had the option of having an additional scan at 6-8 h p.i. Emission scans were acquired in 3D mode at variable times per field of view (3 min on the day of injection, extending to 7 min at 92–148 h). PET/CT scans were performed with low-dose CT for attenuation correction with a single low-dose CT scan at 24 h that was obtained with a 80 mA tube current (120 kVp, estimated radiation dose 9.0 mGy), while all other low-dose CT scans were done with 10 mA current (120 kVp, estimated radiation dose 1.1 mGy). Images were reconstructed with a 70 cm field of view into a 128x128

matrix using iterative ordered subset expectation maximization (OSEM: 16 subsets; 2 iterations). All corrections per manufacturer were applied.

Uptake in Normal Tissues and Lesions

Images were evaluated visually for sites of ^{89}Zr-IAB22M2C uptake. Volumes of interest (VOI) were drawn on PET/CT images within normal organs or tissues including heart, lung, liver, spleen, bone marrow, nodes, kidney, and tumor lesions using dedicated software (Hermes Medical Solutions, Chicago, IL). A site of uptake that did not conform to normal expected biodistribution and was clearly above the adjacent normal background activity was considered positive for a tumor lesion. A subset of index lesions (maximum of two lesions per patient) was analyzed for uptake trends. Standard uptake value (SUV) was quantified using either mean SUV (normal tissues) or maximum SUV (lesions) normalized to lean body mass (SUV_{LBM}) (*18*).

Serum Clearance Measurements

Multiple blood samples were obtained for assessment, including a baseline sample prior to ^{89}Zr-IAB22M2C infusion, followed by sampling at 5, 30, 60, and 120–240 min p.i., and subsequently at the time of each PET scan, totaling 7-8 samples. Samples were measured in duplicate using a NaI (Tl) gamma well-type detector (Wallac Wizard 1480 automatic gamma counter, Perkin Elmer) together

with appropriate standards. The measured activity concentrations were converted to percent injected activity/liter (% IA/L).

Derivation of Whole-body and Serum Clearance

In order to visualize trends in biodistribution and pharmacokinetics, we examined the time course of whole-body and serum activity clearance together with SUV for normal tissues and lesions.

RESULTS

A total of six patients were imaged in this initial dose escalation phase (Table 1). Injections were tolerated well, with no infusion reaction seen in any patients. No adverse events were observed over the study period for any patients. The mean (range) injected activity was 108 (92–120) MBq (2.91 (2.5–3.25) mCi). The radiolabeled antibody mass was 0.12 mg for the 0.2 mg dose level and for other levels, the mean (± SD) mass was 0.34 (± 0.02) mg.

Biodistribution

Prominent activity was seen in the spleen, bone marrow, and liver in all patients; the highest uptake was seen in the spleen, followed by marrow. Blood

pool activity was negligible at the lowest minibody mass and was increasingly seen at early and later time points with higher minibody mass (Fig. 1). Uptake in liver was noted in all patients and GI tract activity (on average, 4.5% of injected activity) was seen up to 48 h p.i. The gall bladder was frequently visualized at the earliest times, with peak activity on the first or second day. Renal uptake varied among patients but was primarily cortical and tended to plateau beyond 48 h. No significant bladder activity was seen except in one patient (1.0 mg), in which activity was clearly seen in the urinary bladder in both of the early scans. The biodistribution of ^{89}Zr-IAB22M2C was highly dependent on minibody mass (Fig. 2). At the lowest mass dose (0.2–0.5 mg), uptake was almost completely confined to the spleen and, to a lesser extent, bone marrow and lymph nodes with little or no apparent blood pool activity even at the earliest times p.i. As the mass dose increased, blood pool retention increased and the biodistribution showed higher liver uptake at later times. However, spleen uptake remained dominant at all times for all minibody masses examined.

Serum and Whole-body Kinetics

Serum clearance was bi-exponential and was dependent on the mass of minibody administered. At lower masses (0.2–1.5 mg), activity in the serum cleared very rapidly (Fig. 3A). The effective half-times ranged between 0.3–10.6 h for the fast component and between 26.4–102.7 h for the slow component.

Whole-body clearance generally conformed to monoexponential kinetics with the exception of the 1.0 mg minibody mass, for which it was distinctly bi-exponential (Fig. 3B). The median whole-body biological half-life ($T_{1/2}b$) was 235 h (range 123–288 h) and had no obvious relationship with minibody mass, apart from the idiosyncratic fast clearance in the patient receiving the 1.0 mg dose.

Uptake in Normal Tissues

The highest uptake was seen in the spleen in all patients at all minibody dose levels but with a consistent pattern of decreasing uptake at higher cold minibody masses (Fig. 2, Fig. 4, A-D). For low minibody masses, spleen uptake was maximal in the earliest images and subsequently decreased, while for the two highest masses (5 and 10 mg) maximal uptake occurred at about 24 h. The range of splenic SUV_{LBM} (Fig. 4A) extended from 10.5 for the 10 mg dose to 50 for the 0.2 mg dose. Bone marrow showed the second highest uptake, reaching a peak in most patients by 6–24 h. Marrow uptake was also highly dependent on minibody mass, with SUV_{LBM} ranging from 1.8–8.6 for 10 mg to 0.2 mg, respectively (Fig. 4B). Liver uptake was significantly lower than spleen, and was generally highest at the earlier times of imaging on day 1 or within 24 h. Liver uptake generally showed either a mild decrease or plateau over 48–120 h and showed an opposite relation to minibody mass dose such that larger masses (1.0 mg or above) showed

higher uptake (Fig. 4C). Multiple normal nodes were seen in all patients at all dose levels except 1 mg. The greatest number of nodes and highest nodal uptake was noted at 0.2 mg, subsequently decreasing as minibody mass increased (Fig. 4D). Nodal upake increased within the first 24-48 h in most patients, though it did not increase substantially in higher masses. At both 0.2 and 0.5 mg levels, multiple nodes were prominently seen even at the earliest imaging times (2–6 h p.i.). Normalized uptake in organs in relation to muscle uptake is separately provided in Supplementary Figure 1.

Uptake in Metastatic Lesions

Metastatic lesion uptake was prominently noted in two patients (one melanoma and one HCC) imaged at 0.2 and 0.5 mg dose levels, respectively. Both patients were receiving immunotherapy. Lesion uptake was seen as early as 2 h p.i. and gradually increased with delayed imaging; the highest uptake in most lesions was seen at 24 or 48 h. One hepatic metastasis showed the highest uptake at 2–4 h imaging. The patient with melanoma showed uptake in a deltoid muscle metastasis with an SUV of 1.4 that was also FDG-avid and found to have peritumoral and intratumoral CD8 T cell infiltration after surgical excision of the lesion for clinical reasons (Fig. 5). The HCC patient had uptake in two liver metastases (SUVmax of 14.6 and 22.85) and additional uptake in three abdominal lymph node metastases (SUVmax ranging from 5.85–10.9) (Fig. 6). No

significant uptake of ^{89}Zr-IAB22M2C was seen in four patients with lung metastases (SUV of 0.3–1.2).

The uptake in tumors by directed imaging of CD8+ T cells with ^{89}Zr-IAB22M2C PET was both concordant and discordant with FDG PET. In the melanoma patient, the lesions were positive on both ^{89}Zr-IAB22M2C and FDG PET (Fig. 5). Of the four patients with negative ^{89}Zr-IAB22M2C uptake in lesions, a lung metastasis in one patient demonstrated FDG avidity (Fig. 7), while the other three patients had no FDG uptake in any lesions. All four patients had either not initiated immunotherapy (n=1), had received immunotherapy in the past more than six months prior to imaging (n=2), or had been receiving immunotherapy (nivolumab) for about two years (n=1). The ^{89}Zr-IAB22M2C-negative lesions included nodes (1.7-4.0 cm), a soft tissue lesion (3.3 cm), a liver lesion (3.7 cm), and lung nodules (0.5-4.7 cm) (Fig. 7).

DISCUSSION

Immune-modulating checkpoint blockade therapies are increasingly playing a critical role in the treatment of several cancers. While they are being used in the treatment of several cancers and across specific patient populations, response is seen in only a subset of patients. A key determinant of successful therapy is the presence of CD8+ T cells that modulate the immune response. Current methods of assessing CD8+ T cell infiltration by tumor biopsy are

invasive and may not always be practical or available. Additionally, tumor biopsies only assess the single site of sampled disease, which may be problematic given immunologic heterogeneity among multiple tumors within an individual patient (*19*). A noninvasive method of imaging that can accurately allow for assessment of CD8+ T cells in tumors would be extremely useful in clinical research and patient management to better determine the effectiveness of therapy.

This is a first-in-human study using ^{89}Zr-IAB22M2C, a novel and unique minibody that is highly specific for targeting CD8+ T cells, that shows clinical feasibility in PET/CT imaging. We evaluated ^{89}Zr-IAB22M2C PET imaging as a means to assess CD8+ T cell distribution in normal and malignant tissues and studied its distribution and kinetics in patients with a variety of malignancies. In this unique non-invasive whole-body PET study, ^{89}Zr-IAB22M2C was shown to be easy to administer and well tolerated, with no observed infusion-related side effects for any minibody mass level mass up to 10 mg.

The biodistribution of ^{89}Zr-IAB22M2C is strongly suggestive of targeting CD8+ T cell-enriched tissues; notably high uptake was seen in spleen, bone marrow, and lymph nodes. The time course of activity seen in the gall bladder and GI tract was consistent with metabolic excretion via the hepatobiliary pathway, as noted with other ^{89}Zr-labeled minibodies (*13*). Liver and kidneys were other tissues with notable uptake, with accumulation in kidney primarily confined to the renal cortex. However, in one patient who received a 1.0 mg minibody mass,

there was early urinary clearance with significant activity in the urinary bladder at both the 2–4 h and 6–8 h time points. This observation, coupled with an unusual whole-body clearance curve that was distinctly bi-phasic, is considered to be idiosyncratic. The exact reason for this is unknown and uptake patterns in normal tissues such as bone marrow and spleen in this patient exhibited a similar pattern as in other patients, with good uptake in the CD8+ T cell-rich tissue.

This intial data indicate that the minibody mass influences biodistribution and that targeting of CD8+ T cell-rich tissues such as spleen, bone marrow, and nodes was affected by the minibody mass dose, being highest at the lowest mass (0.2 mg) and lowest at the highest mass (10 mg). This suggests a saturation effect due to competitive binding between the increasing amount of cold minibody and the radiolabeled ^{89}Zr-IAB22M2C. This is supported by the serum clearance data, which shows very rapid extraction of lower minibody masses from the circulation, while slower clearance and higher retention was seen for higher minibody masses (5-10 mg). As the minibody mass increases, accessible antigen sites are saturated, more minibody remains in the circulation, and accumulation in liver gradually increases.

Most radiolabeled minibody appeared to be stably bound to CD8+ T cell-rich tissues over the duration of measurements, as indicated by the lack of any effect of increasing minibody mass on whole-body clearance of activity. The inverse relationship between liver uptake and minibody mass is unclear but may

be affected by longer clearance time. The overall serum clearance was rapid for ^{89}Zr-IAB22M2C, as noted for other minibodies (*13*) (Fig. 3), allowing for earlier optimal localization in normal tissues as well as prominent lesion detection within 6–24 h p.i. (Figs. 5 and 6).

Multiple time point imaging showed variable trends in uptake and retention pattern in different tissues with stable uptake in CD8+ tissues and clearance of blood pool and background activity over time. CD8+ T cell-rich tissue (spleen and marrow) showed the most prominent and stable uptake with time, with high uptake at early times at low minibody masses that tended to plateau beyond 24 h imaging and high retention even at later time points, suggesting minimal recirculation or excretion. Nodal uptake and visualization varied in time with minibody mass change, with more nodes seen at early time points (6–24 h p.i.) at lower mass as compared to higher mass (5 or 10 mg), suggesting a strong effect of the competitive binding of the cold minibody. However, there was an exception seen at the 1 mg level, where lymph nodes did not show significant uptake, possibly related to lower binding due to faster clearance seen in this particular patient. Increased minibody binding to the cells, along with greater clearance of activity from blood and background tissues at later time points, allows for better detection of nodes. The assessment of optimal mass and time for imaging based on the initial results of visual assessment and uptake patterns in tissues and lesions shows that imaging at 24 h p.i. provides good

visualization of both normal and tumor tissues that may be rich in CD8+ T cells. In this report on

Tumor lesions showed variable uptake of ^{89}Zr-IAB22M2C in patients, possibly related to the treatment profile or the variable presence of CD8+ T cells. High and early ^{89}Zr-IAB22M2C uptake was noted in lesions in two patients imaged at lower masses (0.2 and 0.5 mg). These patients were receiving immunotherapy with pembrolizumab and nivolumab (0.2 and 0.5 mg, respectively), suggesting possible modulation of TILs, leading to higher concentration of CD8+ T cells and therefore prominent visualization by ^{89}Zr-IAB22M2C PET/CT imaging. In one patient, histology and immunohistochemistry confirmed suspected CD8+ T cell infiltration in a lesion that had uptake of^{89}Zr-IAB22M2C. Three patients with metastatic lung cancer did not show prominent uptake. While the exact status of TIL is not known due to the absence of parallel biopsy data, we postulate that this may be related to a lack of ongoing treatment with immunotherapy and therefore low TIL. It is also possible that the tumors did not have active disease, as all tumors were also non-FDG-avid in these patients.

^{89}Zr-IAB22M2C PET and FDG PET were concordant in the patient with melanoma (both positive; Fig. 5) and in three patients with lung cancer (both negative). In one patient, for whom immunotherapy was not initiated, FDG was positive while ^{89}Zr-IAB22M2C was negative, possibly because TIL had not been

stimulated at the time of ^{89}Zr-IAB22M2C imaging (Fig. 6). This suggests that ^{89}Zr-IAB22M2C uptake is independent of other processes such as enhanced permeability and vascular flow, which may lead to non-specific uptake in viable tumors.

Due to the small number of patients and variability in tumor types and treatment profiles, differences in lesion uptake among minibody mass doses cannot be established at this time. Our limited assessment suggests a more favorable balance of normal tissue and lesion visualization at lower minibody masses (less than 5 mg). Further analysis is ongoing in additional patients at different mass levels to further establish the role of minibody mass in imaging and dosimetry.

CONCLUSION

This first-in-human study shows that PET imaging with ^{89}Zr-Df-IAB22M2C is safe, feasible, and well tolerated. The data supports the ability of ^{89}Zr-IAB22M2C minibody to successfully target CD8+ T cell-rich tissues. ^{89}Zr-IAB22M2C imaging has favorable kinetics for early imaging within 6–24 h p.i. Further evaluation is underway in more patients and a study incorporating parallel biopsies is accruing patients.

ACKNOWLEDGMENTS

The authors would like to thank Antoni Ribas and Suzanne Topalian for their early contributions to the concept of this study. We also want to posthumously acknowledge Jean Gudas for her contributions to the development of the agent. We thank Dr. Maria Cecilia Lezcano Lopez in MSK's Department of Pathology for providing us with the pathology images of IHC and H&E stained tissues.

Funding Support

This research was supported by ImaginAb, Inc., the Parker Institute for Cancer Immunotherapy, and the Radiochemistry & Molecular Imaging Probe Core of MSK, supported by NIH/NCI Cancer Center Support Grant P30 CA008748.

Disclosure of Potential Conflicts of Interest

NPT serves as a consultant to Y-mAbs Therapeutics, Inc. and has served on the advisory board of Progenics, Bayer, and Actinium Pharma. She has received honoraria from MedImmune/AstraZeneca. She receives or has received research support from Imaginab, Genentech, and Actinium Pharma. MAP has received consulting fees from Bristol-Myers Squibb, Merck, Array BioPharma, Novartis, Incyte, NewLink Genetics, and Aduro Biotech (2015-present); honoraria from Bristol-Myers Squibb and Merck; and institutional support from Rgenix Inc.,

Infinity, Bristol-Myers Squibb, Merck, Array BioPharma, Novartis, and AstraZeneca. MDH receives research funding from Bristol-Myers Squibb; is a paid consultant to Merck, Bristol-Myers Squibb, AstraZeneca, Genentech/Roche, Janssen, Nektar, Syndax, Mirati, and Shattuck Labs; and has received travel support/honoraria from AztraZeneca and BMS. A patent has been filed by MSK related to the use of tumor mutation burden to predict response to immunotherapy (PCT/US2015/062208), which has received licensing fees from PGDx. JJH has received research support and consulting fees from Bristol-Meyers Squibb and consulting fees from Eli Lilly and Company, CytomX Therapeutics, and Eisai Co., Ltd. CAB has received research funding for studies he is leading through his institution within the past year from Merck, Amgen, and Elekta, as well as for a study he is participating in from Bristol-Myers Squibb. He served as an unpaid member of an advisory board for Regeneron within the past year and as a paid member of an advisory board for Pfizer and Novartis over two years ago. TCM has received honoraria from Merck, Bristol-Myers Squibb, Incyte, Regeneron, and Aduro. With regard to this publication, JSL's laboratory has received research support from ImaginAb, Inc. U.S. AMW is a board member and consultant to ImaginAb, Inc. JDW reports personal fees from Adaptive Biotech, Advaxis, Amgen, Apricity, Array BioPharma, Ascentage Pharma, Astellas, Bayer, Beigene, Celgene, Chugai, Elucida, Eli Lilly, F Star, Imvaq, Janssen, Kleo Pharma, Linneaus, Merck, Neon Therapeutics, Ono Pharmaceuticals, Polaris Pharma,

Polynoma, Psioxus, Puretech, Recepta, Sellas Life, Serametrix, Surface Oncology, Syndax, and Esanex; and grants and personal fees from Bristol Myers Squibb, Genentech, and MedImmune outside the submitted work. In addition, Dr. Wolchok has pending patents for: Xenogeneic DNA Vaccines with royalties paid to Merial, Alphavirus Replicon Particles Expressing TRP2, Newcastle Disease Viruses For Cancer Therapy, Genomic Signature to Identify Responders to Ipilimumab in Melanoma, Engineered Vaccinia Viruses for Cancer Immunotherapy (to Imvaq), Anti-CD40 Agonist mAb Fused to Monophosphoryl Lipid A (MPL) for Cancer Therapy, and CAR+ T Cells Targeting Differentiation Antigens as Means to Treat Cancer. He also has the following patents: Myeloid-derived Suppressor Cell (MDSC) Assay with royalties paid to Serametrix, Anti-PD1 Antibody licensed to Agenus, Anti-GITR Antibodies and Methods of Use Thereof licensed to Agenus/Incyte, and Anti-CTLA4 Antibodies licensed to Agenus. JDW also has equity in: Potenza Therapeutics, Tizona Pharmaceuticals, Adaptive Biotechnologies, Elucida, Imvaq, Beigene, Trieza, and Linneaus. Additionally, The Parker Institute is a shareholder of ImaginAb and has partnered with ImaginAb to directly support this clinical research at MSK. No other potential conflicts of interest relevant to this article exist.

KEY POINTS

QUESTION: Is it feasible to non-invasively visualize CD8 T cells with ^{89}Zr-IAB22M2C?

PERTINENT FINDINGS: This phase I study evaluated the safety, feasibility, and optimal mass dose of imaging with a novel anti-CD8 minibody (^{89}Zr-IAB22M2C) and performed a preliminary evaluation of the ability of ^{89}Zr-IAB22M2C to target CD8+ T cell-rich tissues in patients with a variety of solid tumors. Preliminary data is encouraging, as ^{89}Zr-IAB22M2C was safe and allows early imaging of CD8+ T cell-rich tissues at 24 h post-injection; a phase II study to evaluate the concordance of ^{89}Zr-IAB22M2C imaging with CD8+ T cell presence by standard histologic assessment in patients receiving immunotherapy is underway.

IMPLICATIONS FOR PATIENT CARE: If proven in subsequent studies, ^{89}Zr-IAB22M2C imaging has the potential to non-invasively assess the presence of CD8+ T cells in patients' tumors, which may ultimately serve as a biomarker of immunotherapy outcome and inform clinical trials of novel immunotherapies that act mechanistically through the presence of CD8+ T cells.

REFERENCES

1. Gooden MJ, de Bock GH, Leffers N, Daemen T, Nijman HW. The prognostic influence of tumour-infiltrating lymphocytes in cancer: a systematic review with meta-analysis. *Br J Cancer.* 2011;105:93-103.

2. Azimi F, Scolyer RA, Rumcheva P, et al. Tumor-infiltrating lymphocyte grade is an independent predictor of sentinel lymph node status and survival in patients with cutaneous melanoma. *J Clin Oncol.* 2012;30:2678-2683.

3. Brahmer JR. PD-1-targeted immunotherapy: recent clinical findings. *Clin Adv Hematol Oncol.* 2012;10:674-675.

4. Tumeh PC, Harview CL, Yearley JH, et al. PD-1 blockade induces responses by inhibiting adaptive immune resistance. *Nature.* 2014;515:568-571.

5. Ribas A, Dummer R, Puzanov I, et al. Oncolytic Virotherapy Promotes Intratumoral T Cell Infiltration and Improves Anti-PD-1 Immunotherapy. *Cell.* 2018;174:1031-1032.

6. Brahmer JR, Tykodi SS, Chow LQ, et al. Safety and activity of anti-PD-L1 antibody in patients with advanced cancer. *N Engl J Med.* 2012;366:2455-2465.

7. Topalian SL, Hodi FS, Brahmer JR, et al. Safety, activity, and immune correlates of anti-PD-1 antibody in cancer. *N Engl J Med.* 2012;366:2443-2454.

8. Tavare R, Escuin-Ordinas H, Mok S, et al. An Effective Immuno-PET Imaging Method to Monitor CD8-Dependent Responses to Immunotherapy.

Cancer Res. 2016;76:73-82.

9. Tavare R, McCracken MN, Zettlitz KA, et al. Engineered antibody fragments for immuno-PET imaging of endogenous CD8+ T cells in vivo. *Proc Natl Acad Sci U S A.* 2014;111:1108-1113.

10. Pandit-Taskar N, O'Donoghue JA, Durack JC, et al. A Phase I/II Study for Analytic Validation of 89Zr-J591 ImmunoPET as a Molecular Imaging Agent for Metastatic Prostate Cancer. *Clin Cancer Res.* 2015;21:5277-5285.

11. Knowles SM, Wu AM. Advances in immuno-positron emission tomography: antibodies for molecular imaging in oncology. *J Clin Oncol.* 2012;30:3884-3892.

12. Olafsen T, Sirk SJ, Olma S, Shen CK, Wu AM. ImmunoPET using engineered antibody fragments: fluorine-18 labeled diabodies for same-day imaging. *Tumour Biol.* 2012;33:669-677.

13. Pandit-Taskar N, O'Donoghue JA, Ruan S, et al. First-in-Human Imaging with 89Zr-Df-IAB2M Anti-PSMA Minibody in Patients with Metastatic Prostate Cancer: Pharmacokinetics, Biodistribution, Dosimetry, and Lesion Uptake. *J Nucl Med.* 2016;57:1858-1864.

14. Tove Olafsen ZKJ, Jason Romero, Charles Zamilpa, Filippo Marchioni, Green Zhang, Michael Torgov, Daulet Satpayev and Jean M. Gudas. Abstract LB-188: Sensitivity of 89Zr-labeled anti-CD8 minibody for PET imaging of infiltrating CD8+ T cells. *AACR.* 2016;Proceedings of the 107th Annual Meeting

of the American Association for Cancer Research; 2016 Apr 16-20; New Orleans, LA. Philadelphia (PA): AACR; Cancer Res 2016;76(14 Suppl):Abstract nr LB-188.

15. Holland JP, Caldas-Lopes E, Divilov V, et al. Measuring the pharmacodynamic effects of a novel Hsp90 inhibitor on HER2/neu expression in mice using Zr-DFO-trastuzumab. *PLoS One.* 2010;5:e8859.

16. Holland JP, Divilov V, Bander NH, Smith-Jones PM, Larson SM, Lewis JS. 89Zr-DFO-J591 for immunoPET of prostate-specific membrane antigen expression in vivo. *J Nucl Med.* 2010;51:1293-1300.

17. Holland JP, Sheh Y, Lewis JS. Standardized methods for the production of high specific-activity zirconium-89. *Nucl Med Biol.* 2009;36:729-739.

18. Morgan DJ, Bray KM. Lean body mass as a predictor of drug dosage. Implications for drug therapy. *Clin Pharmacokinet.* 1994;26:292-307.

19. Reuben A, Spencer CN, Prieto PA, et al. Genomic and immune heterogeneity are associated with differential responses to therapy in melanoma. *NPJ Genom Med.* 2017;2.

20. Borjesson PK, Jauw YW, de Bree R, et al. Radiation dosimetry of 89Zr-labeled chimeric monoclonal antibody U36 as used for immuno-PET in head and neck cancer patients. *J Nucl Med.* 2009;50:1828-1836.

FIGURES AND TABLES

Table 1. Patient Demographics

Total patients	6
Age	38–81 years
Sex	
Male	3
Female	3
Primary malignancy	
Melanoma	1
Hepatocellular carcinoma	1
Lung	4
Treatment profile for current immunotherapy	Patients
None	1
Current <1 month	1
Current >6 months	2
Prior >6 months from imaging	2

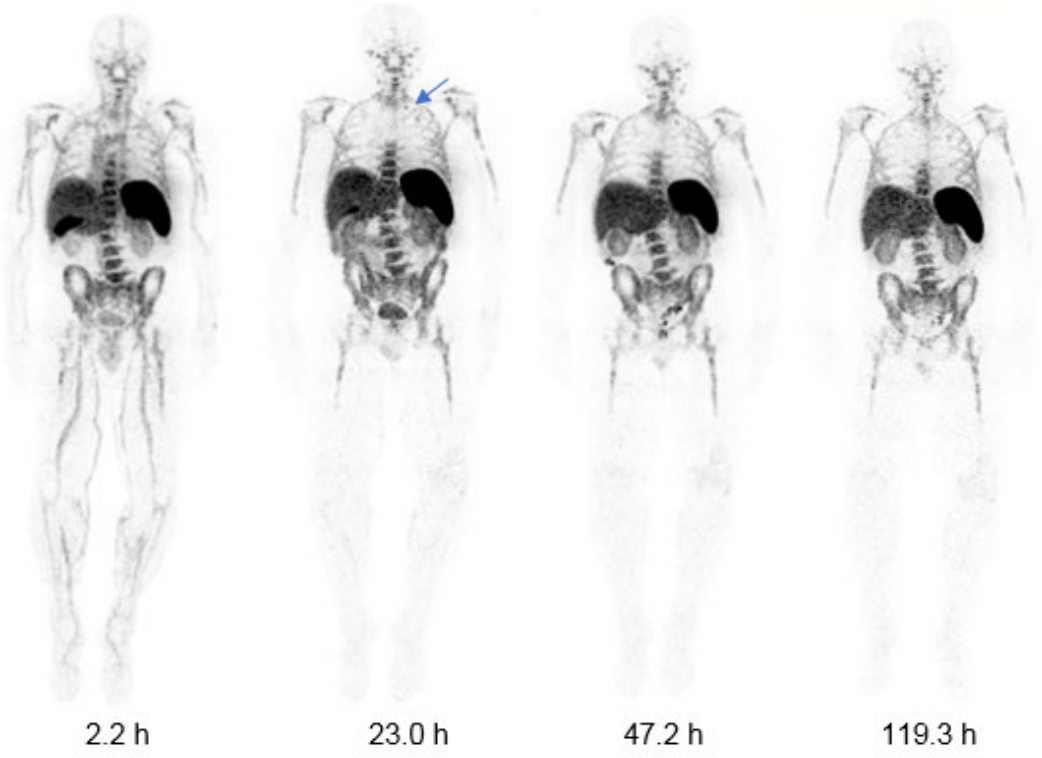

Figure 1. Biodistribution: Whole-body images at various times of imaging in a single patient (1.5 mg minibody dose). All images show most intense activity within spleen, followed by marrow, liver, and kidneys. Uptake within normal nodes was also visualized by 23 h (arrow).

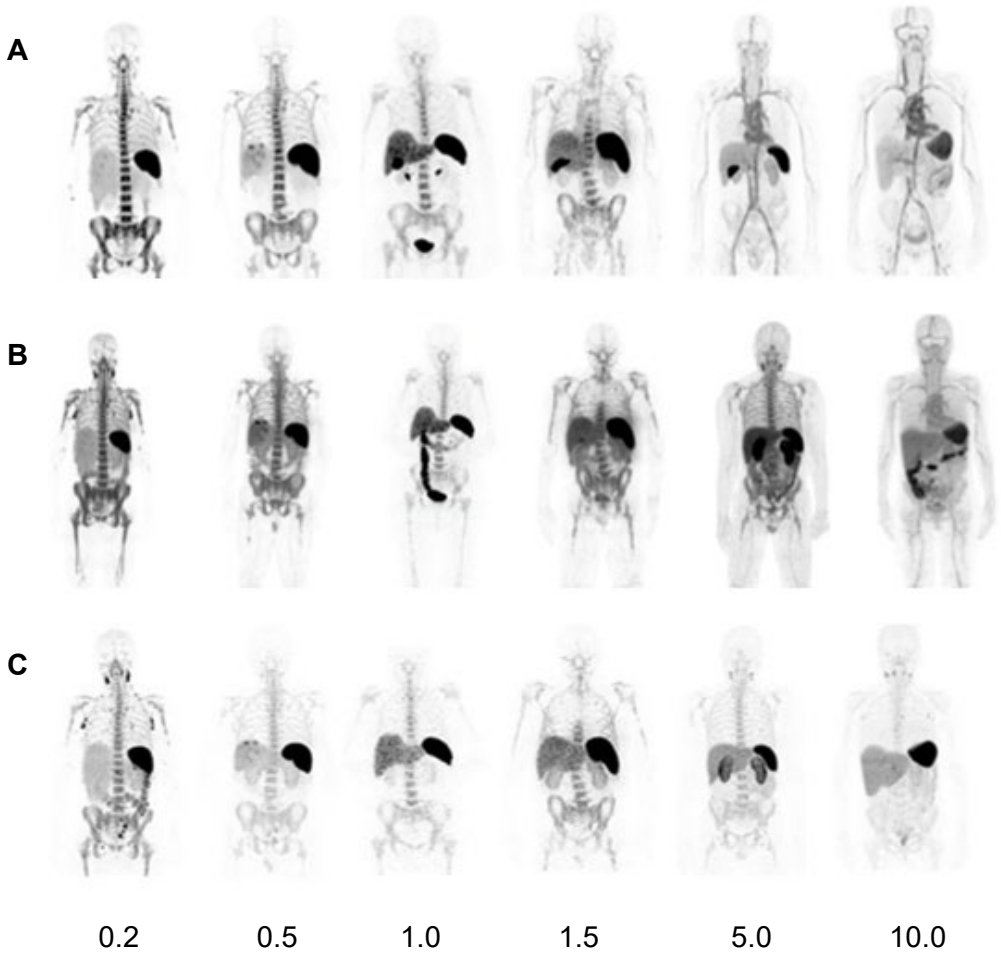

Figure 2. Biodistribution and normal organ uptake in six patients at 2–4 h (A), 24 h (B), and 92–148 h (C) post-injection of ^{89}Zr-IAB22M2C at different minibody masses (in mg).

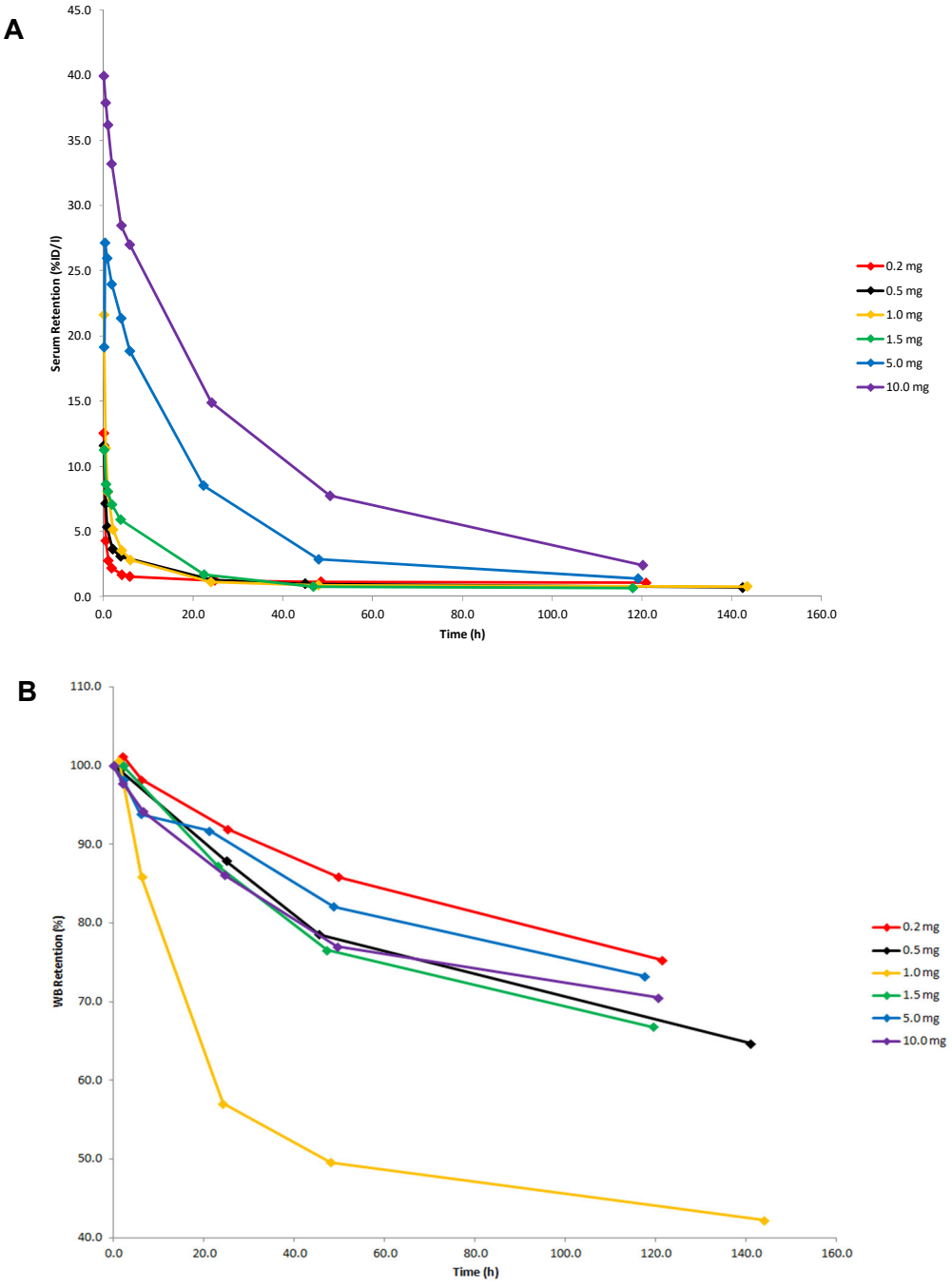

Figure 3. Serum (A) and whole-body clearance (B) of ^{89}Zr-IAB22M2C at various mass levels, in aggregate mean values of decay-corrected activity retention.

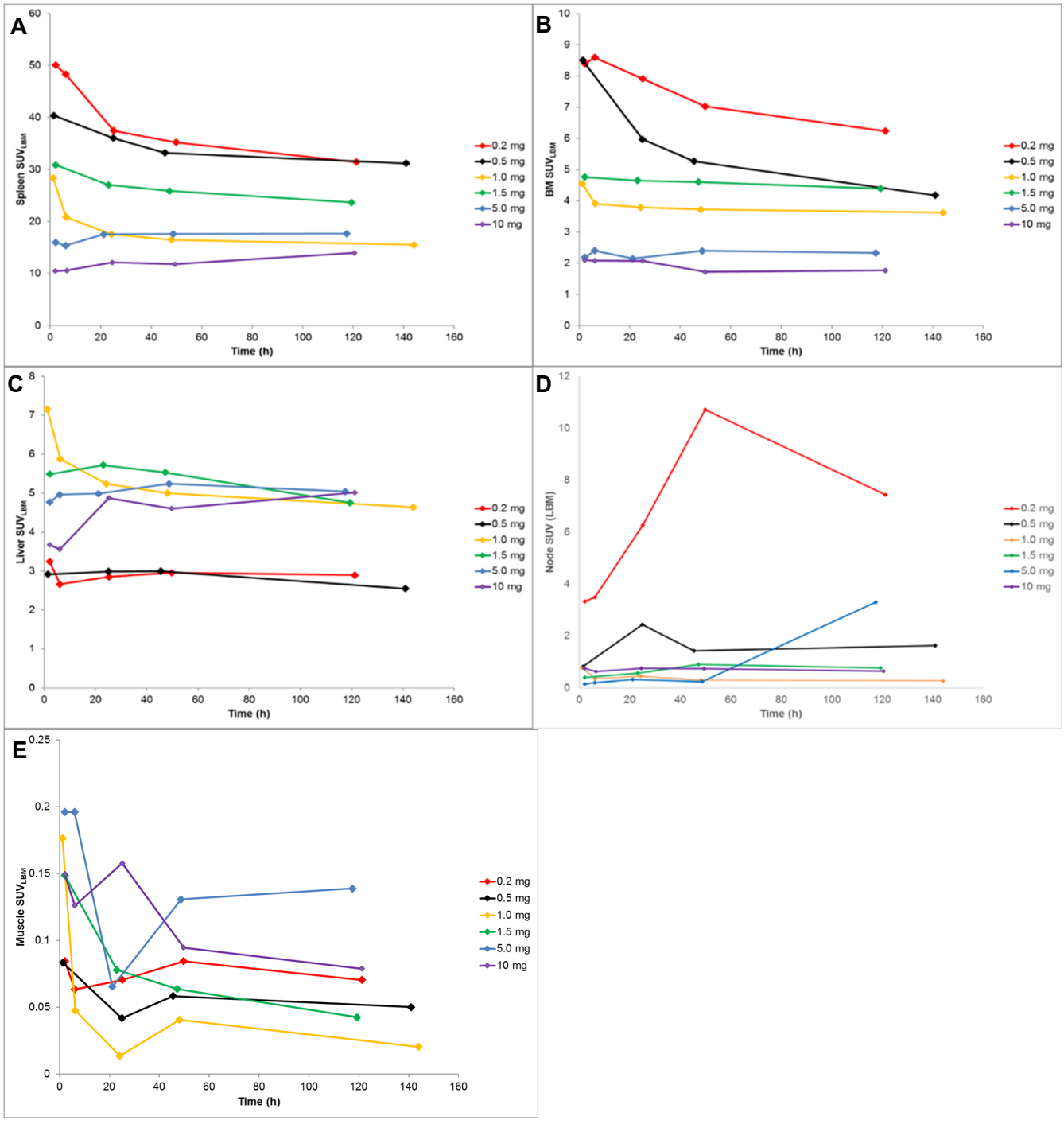
A
Spleen SUV$_{LBM}$
Time (h)
0.2 mg
0.5 mg
1.0 mg
1.5 mg
5.0 mg
10 mg
B
BM SUV$_{LBM}$
Time (h)
0.2 mg
0.5 mg
1.0 mg
1.5 mg
5.0 mg
10 mg
C
Liver SUV$_{LBM}$
Time (h)
0.2 mg
0.5 mg
1.0 mg
1.5 mg
5.0 mg
10 mg
D
Node SUV (LBM)
Time (h)
0.2 mg
0.5 mg
1.0 mg
1.5 mg
5.0 mg
10 mg
E
Muscle SUV$_{LBM}$
Time (h)
0.2 mg
0.5 mg
1.0 mg
1.5 mg
5.0 mg
10 mg

Figure 4. Normal organ uptake (SUVmean LBM) in (A) spleen, (B) marrow, (C) liver, (D) nodes, and (E) muscle (background uptake) versus minibody mass.

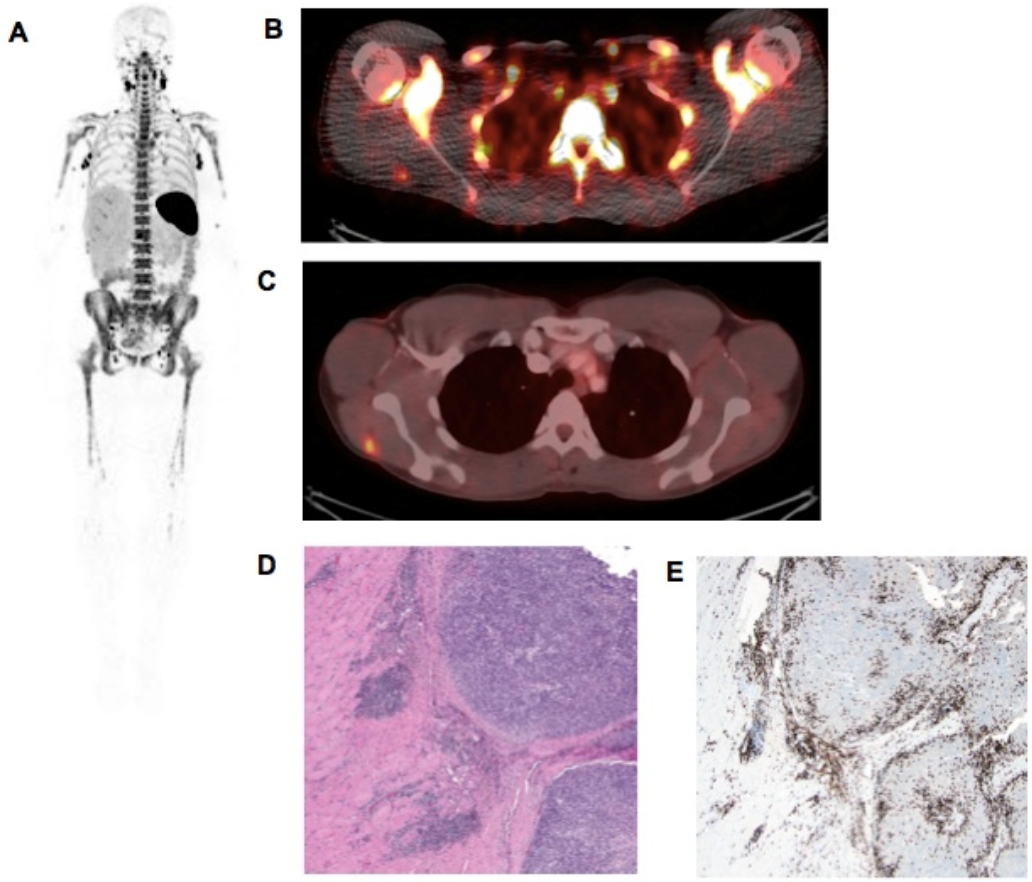

Figure 5. A 24-hour whole-body (MIP) image in a patient imaged with 0.2 mg of ^{89}Zr-IAB22M2C. Intense uptake is noted in lymph nodes (A). Fusion image at 24 h shows ^{89}Zr-IAB22M2C uptake in lesion in deltoid (B), which was also FDG-positive (C). H&E shows melanoma tumor nodules on the right within skeletal muscle (D) and immunohistochemistry (E) highlights the presence of CD8+ T cells at the periphery and infiltrating into the tumor.

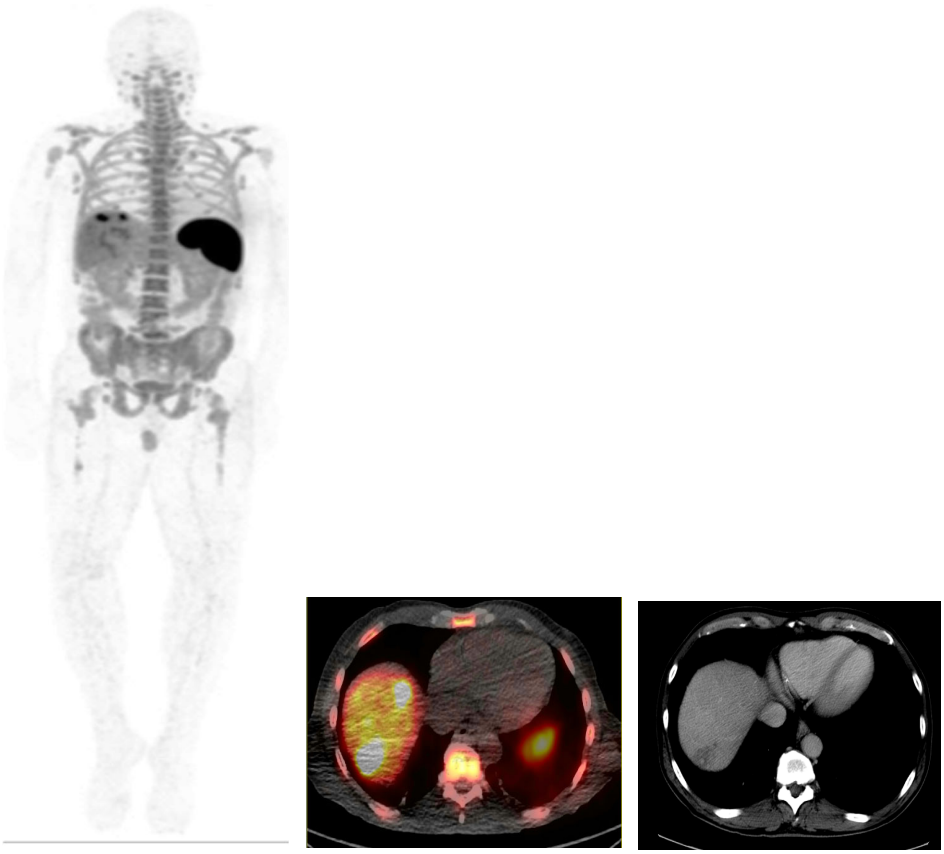

Figure 6. Whole-body (MIP) image of patient with Hepatocellular carcinoma imaged with 0.5 mg of ^{89}Zr-IAB22M2C. Images show ^{89}Zr-IAB22M2C positive lesions in two liver metastases (SUVmax of 14.6 and 22.85) and additional uptake in three abdominal lymph node metastases (SUVmax ranging from 5.85–10.9).

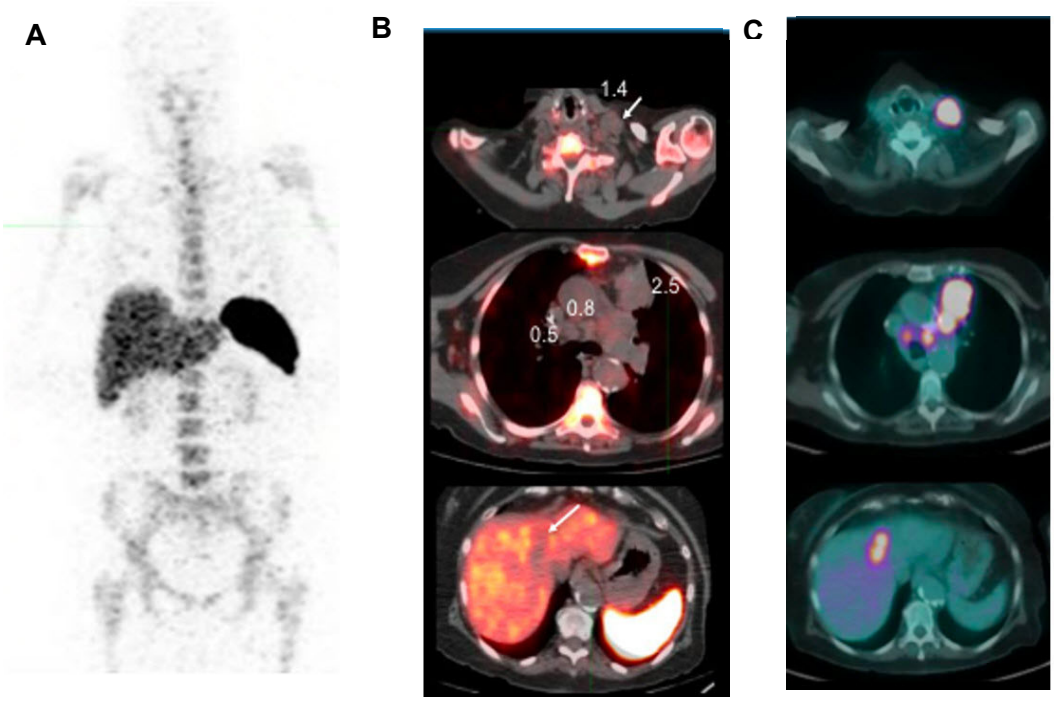

Figure 7. Whole-body (MIP) image (A) of patient with lung cancer not initiated on immunotherapy who was imaged with 1.0 mg of ^{89}Zr-IAB22M2C (B). Images show FDG-positive lesions (C) in left neck (SUVmax 17.8; 3.2cm), mediastinum (SUVmax 11.1; 2.2 cm), left upper lobe (SUVmax 20.4; 4.7 cm), and liver (SUVmax 11.6; 3.7 cm), which did not show uptake of ^{89}Zr-IAB22M2C (B).

SUPPLEMENTAL DATA

Supplementary Figure 1. Normal organ uptake in (A) spleen; (B) bone marrow; (C) liver; (D) aorta; (E) kidney; and (F) lung at different minibody masses. The y-axis represents the ratio of SUVmean of reference organs to SUVmean muscle per LBW.

A

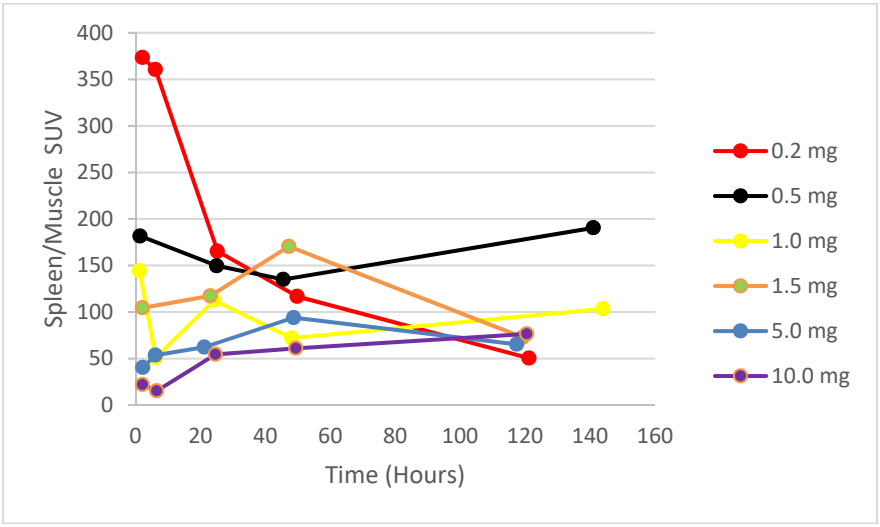

B

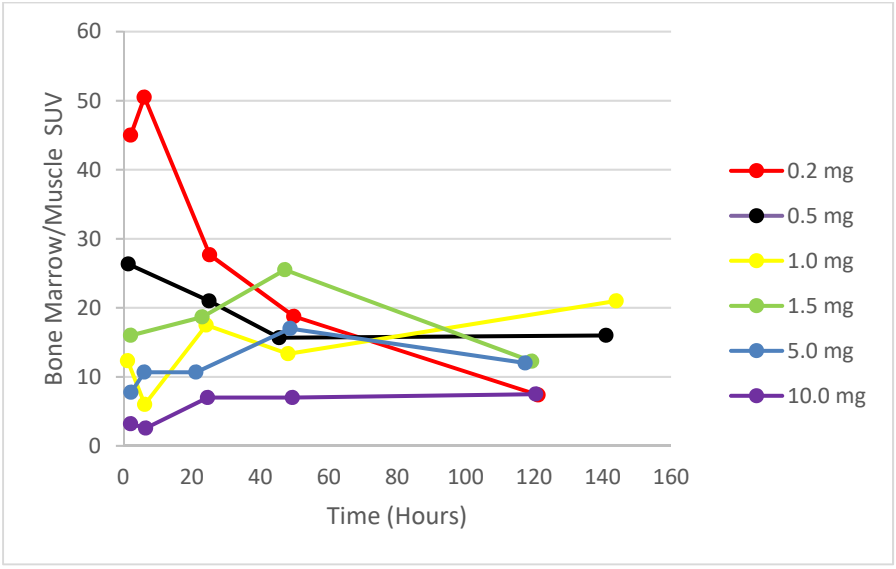

C

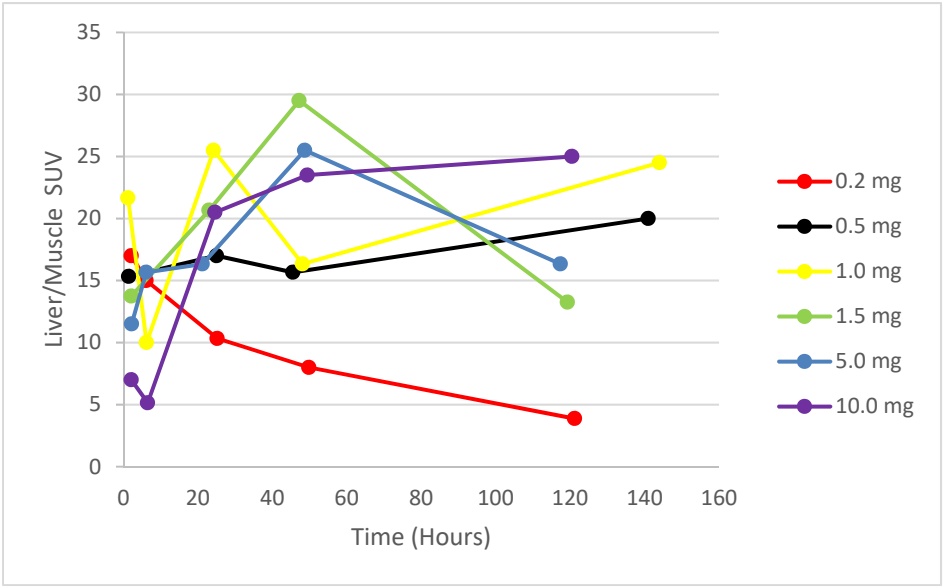
35
30
25
20
15
10
5
0
Liver/Muscle SUV
0
20
40
60
80
100
120
140
160
Time (Hours)
0.2 mg
0.5 mg
1.0 mg
1.5 mg
5.0 mg
10.0 mg

D

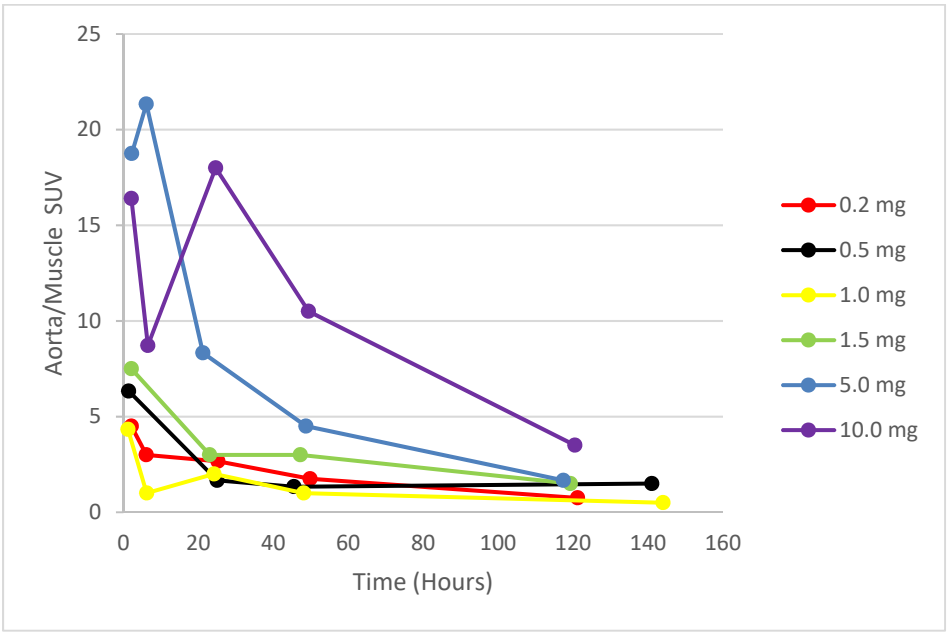
25
20
15
10
5
0
Aorta/Muscle SUV
0
20
40
60
80
100
120
140
160
Time (Hours)
0.2 mg
0.5 mg
1.0 mg
1.5 mg
5.0 mg
10.0 mg

E

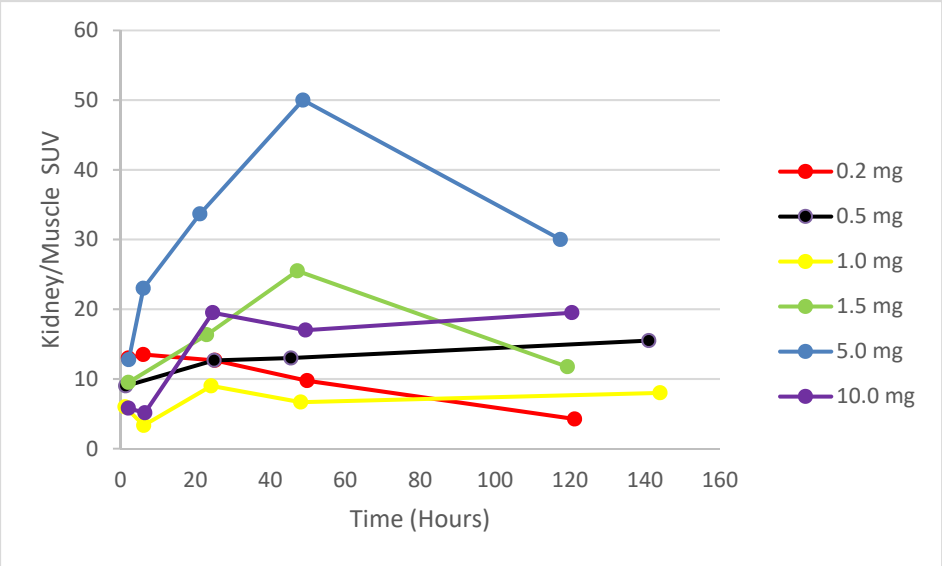
Kidney/Muscle SUV
60
50
40
30
20
10
0
0
20
40
60
80
100
120
140
160
Time (Hours)
0.2 mg
0.5 mg
1.0 mg
1.5 mg
5.0 mg
10.0 mg

F

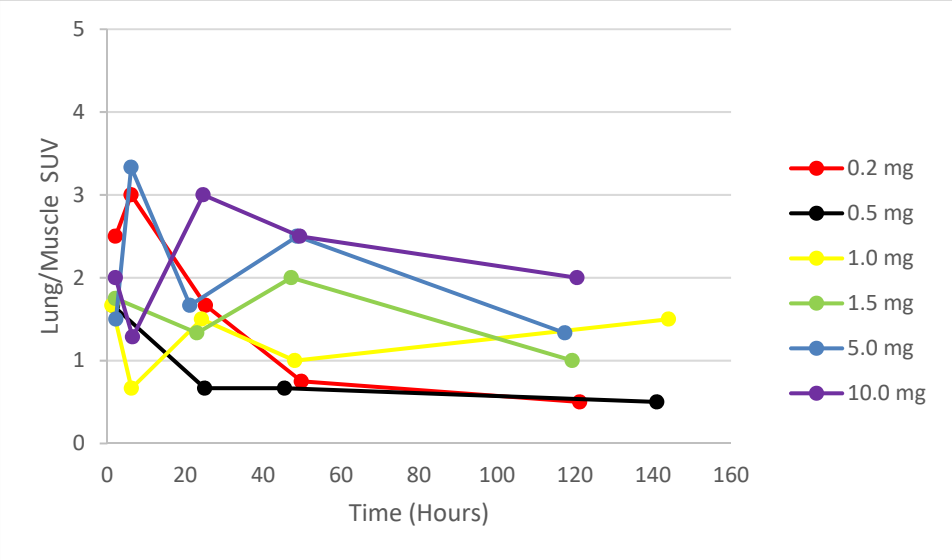
Lung/Muscle SUV
5
4
3
2
1
0
0
20
40
60
80
100
120
140
160
Time (Hours)
0.2 mg
0.5 mg
1.0 mg
1.5 mg
5.0 mg
10.0 mg